Electronic Supplementary Material (ESI) for Analyst.

Ru(II)-Fe(III) Bimetallic Complex as a Multifunctional Device for Detecting, Signal Amplifying, and Degrading Oxalate

Supporting information

Cheuk-Fai Chow *[a,b], Pui-Yu Ho[a,b], Cheng-Bin Gong[c].

[a]Department of Science and Environmental Studies, The Hong Kong Institute of Edcuation,10 Lo Ping Road, Tai Po, New Territories, H.K. SAR, China.

[b]Centre for Education in Environmental Sustainability, The Hong Kong Institute of Education, 10 Lo Ping Road, Tai Po Hong Kong SAR, China.

[c]College of Chemistry and Chemical Engineering, Southwest University, Chong Qing, China.

E-mail: cfchow@ied.edu.hk; Fax: (+852) 29487676; Tel: (+852) 29487671

Methods

Materials and General Procedures. 4,4'-Di-*tert*-butyl-2,2'-bipyridine (^{t}Bubpy), $RuCl_3 \cdot 3H_2O$, potassium acetate, sodium L-tartrate dibasic dehydrate, KN_3, KNO_3, KSCN, KH_2PO_4, KBr, KCl and K_2SO_4 were obtained from Aldrich. Potassium oxalate was obtained from Farco chemical supplies. Anhydrous $FeCl_3$, glyoxylic acid monohydrate, pyruvic acid, tetra-*n*-butylammonium hexafluorophosphate and KCN were obtained from Acros. $K_2[Ru(^t Bubpy)(CN)_4]$ was synthesized according to literature method.[1] All solvents used were of analytical grade.

Physical Measurements and Instrumentation. The ^{1}H-NMR spectra were recorded using a Bruker AVANCE III System 400MHz NMR spectrometer. The electrospray mass spectra (ESI-MS) were measured with an AB SCIEX API 2000 LC/MS/MS system. The elemental analyses were performed on a Vario EL CHN analyzer. The infrared spectra in the range 500-4000 cm^{-1} in KBr plates were recorded on a Perkin Elmer Model Frontier FTIR spectrometer and the UV-vis spectra were measured on a Cary 50 ultraviolet visible spectrophotometer. The emission spectra were recorded using a Horiba FluoroMax-4 spectrofluorimetric with a 5 nm slit width and a 0.5 s integration time. Luminescence quantum yields were measured by the optical dilution method[2] using an aerated aqueous solution of $[Ru(bpy)_3]Cl_2$ (φ = 0.028, excitation wavelength at 455 nm)[3] as the standard solution. Cyclic voltammetries were measured on an eDAQ EChem System. Dissolved organic carbon was recorded using a Shimadzu TOC-L CSH High-Sensitivity Total organic Analyzer.

UV-vis Spectroscopic and Spectrofluorimetric Titrations. All solvents used in UV-vis spectroscopic and spectrofluorimetric titrations were KCl/HCl pH 1.5 (0.5M) buffer. Measurements were taken after equilibrium had been reached between the receptor and substrate. A receptor -substrate interaction was analyzed according to Benesi-Hildebrand equations[4] for UV-vis spectroscopic titration (eqn. 1 and 3) or spectrofluorimetric titration (eqn. 2 and 4).

$$\frac{A_O}{A - A_O} = \left(\frac{\varepsilon_o}{\varepsilon_o - \varepsilon}\right)\left(\frac{1}{K_{overall}[substrate]} + 1\right) \quad -------- \quad (1)$$

$$\frac{I_O}{I - I_O} = \left(\frac{a}{b - a}\right)\left(\frac{1}{K_{overall}[substrate]} + 1\right) \quad -------- \quad (2)$$

$$\frac{A_O}{A - A_O} = \left(\frac{\varepsilon_o}{\varepsilon_o - \varepsilon}\right)^2 \left(\frac{1}{K_{Overall}[substrate]^2} + 1\right) \quad -------- \quad (3)$$

$$\frac{I_O}{I - I_O} = \left(\frac{c}{d - c}\right)^2 \left(\frac{1}{K_{overall}[substrate]^2} + 1\right) \quad -------- \quad (4)$$

A_0 and A are the absorbance of the chromogenic reagent in the absence and presence of the substrate; ε_0 and ε are the corresponding molar absorption coefficients of the chromogenic reagent in the absence and presence of the substrate. I_0 and I are luminescence intensity of the fluorogenic reagent in the absence and presence of the substrate; *a, b, c* and *d* are constants; [substrate] is the concentration of target analyte. Formation constants ($K_{overall}$) were estimated from the ratio between the *y*-intercept and the slope of straight lines obtained by plotting $A_0/(A - A_0)$ or $I_0/(I - I_0)$ *vs.* 1/[substrate] or 1/[substrate]^2 depending on 1:1 or 1:2 host-guest interaction respectively. Energies of formation (ΔG/kJ mol^{-1}) of the donor–acceptor ensembles and the acceptor metal–analyte adducts were evaluated from the corresponding formation constants as stated in eqn. (5)[4]: R is the gas constant. T is the temperature at which the experiments conducted.

$$\Delta G = -RT\,In(K_{overall}) \quad -------- \quad (5)$$

Job's Plot. A series of $FeCl_3$ solutions were mixed with $K_2Ru(^tBubpy)(CN)_4$ solutions under the condition that the sum of the concentration of the $FeCl_3$ and $K_2Ru(^tBubpy)(CN)_4$ solutions is constant. Spectral changes (A/A_0) at 606 nm of the resulting mixtures were plotted as a function of mole fraction of $FeCl_3$. All the measurements were carried out in deionized water.

Formation Constants of $[Ru^{II}(^tBubpy)(CN)_4]_2$–$[Fe^{III}(H_2O)_3Cl]_2$ Adducts. UV-vis spectroscopic titrations of solutions of $K_2Ru(^tBubpy)(CN)_4$ (4.76×10^{-4} M) by $FeCl_3$ (0 to 4.76×10^{-4} M) were carried out in a 2:1 ratio of ethanol/pH 1.5 aqueous buffer mixture. Observed absorbance of the resultant mixtures was measured. Formation constant of the $[Ru^{II}(^tBubpy)(CN)_4]_2$–$[Fe^{III}(H_2O)_3Cl]_2$ adducts was analyzed by fitting the titration curves with the 1:1 Benesi-Hildebrand equation (eqn. 1).

Formation Constants of [$FeCl_3$]-[analyte] Adducts. UV-vis spectroscopic or spectrofluorimetric titrations of solutions of $FeCl_3$ (1.67×10^{-4} M) by oxalate (0 to 1.67×10^{-3} M), and those of $FeCl_3$ (3.33×10^{-4} M) by other analytes, i.e. glyoxylic acid (0 to 6.67×10^{-3} M), L-tartrate (0 to 6.67×10^{-3} M), pyruvate, acetate, NCS^-, $H_2PO_4^-$, Br^-, Cl^-, NO_3^-, N_3^- and SO_4^{2-} were carried out in a pH 1.5 aqueous buffer. Observed absorbance or emission of the resultant mixtures was measured. Formation constants of the [$FeCl_3$]-[analyte] adducts were analyzed by fitting the titration curves with the Benesi-Hildebrand equation (eqn. 1, 2 or 3).

Method Detection Limits of Complex 1 toward Oxalate. A series of oxalate (0 to 9.52×10^{-3} M) were mixed with complex **1** solutions (2.17×10^{-4} M). The detection limit studies were carried out in a 2:1 ratio of ethanol/pH 1.5 aqueous buffer mixture at room temperature. Spectroscopic and spectrofluorimetric changes of the resultant mixtures were recorded. Method detection limits were calculated through Hubaux and Vos method.[5]

In Vivo **Toxicity Assay of Complex 1 toward Japanese Medaka (*Oryzias latipes)*** Medaka embryos were obtained from Dr. Doris W. T. Au (City University of Hong Kong). Hatched larvae were maintained in an embryo rearing medium[6], at pH 7.2, and fed with finely ground Otohime BETA1 (Nisshin Co., Japan). Larvae (ca. 4 – 5 mm in length) were fasted for 5 h and then exposed to complex **1** at 5 day-post-hatch (dph) on multiwell cell culture plates. Seven medaka larvae were held in each of the cell culture well. These larvae were incubated in 7 mL of embryo rearing medium, at room temperature, with a suspension of the complex **1** of known concentration, i.e., 0 (as a control), 1, 10 and 100 mg/mL, and were fed every other day, continuously for up to 7 days. The relatively low specific gravity, with respect to water, of complex **1** allowed its solid powders to float/suspend in the embryo-rearing medium rather than sunk to the bottom of the wells. Their vitality was checked every 24 h. Data processing refers to the software of SPSS 21.0.

Reference

1. (a) Demas, J. N.; Turner, T. F.; Crosby, G. A. *Inorg. Chem.* **1969**, 8, 674. (b) Krause, R. A. *Inorg. Chim. Act.* **1977**, 22, 209. (c) Kato, M.; Yamauchi, S.; Hirota, N. *J. Phys. Chem.* **1989**, 93, 3422.
2. J. N. Demas and G. A. Crosby, *J. Phys. Chem.*, **1971**, *75*, 991.
3. K. Nakamaru, *Bull. Chem. Soc. Jpn.*, **1982**, *55*, 2697.
4. Connors, K. A. *Binding Constants, The Measurement of Molecular Complexes Stability*, John Wiley and Sons: New York, 1987.

5. Hubaux, A.; Vos, G. *Anal. Chem.*, **1970**, *42*, 849.
6. Hardman, R. C.; Volz, D. C.; Kullman, S. W.; Hinton, D. E. *Anatom. Record Adv. Integr. Anatom. Evolut. Biol.* **2007**, *290*. 770.

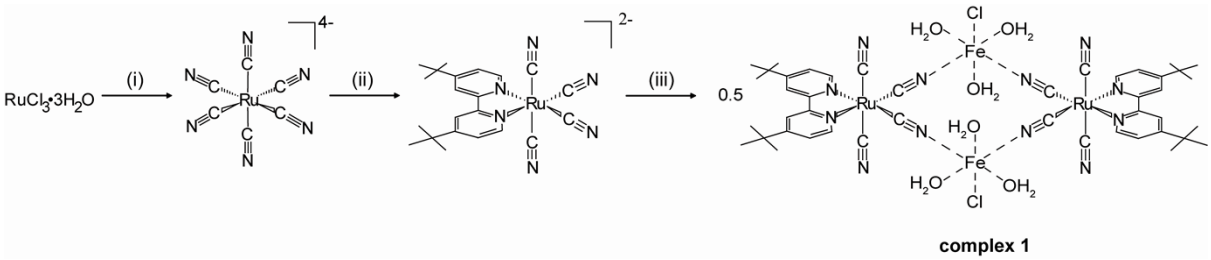

SI. Scheme 1. Schematic diagram of the synthesis of the tetranuclear complex **1**. Reaction condition: (i) reflux with excess amount of KCN in water, (ii) reflux with 1 eqv. mole of ^{t}Bubpy in aqueous methanol (pH 2), (iii) stirring 1 eqv. mole of $FeCl_3$ in deionized water in rtm.

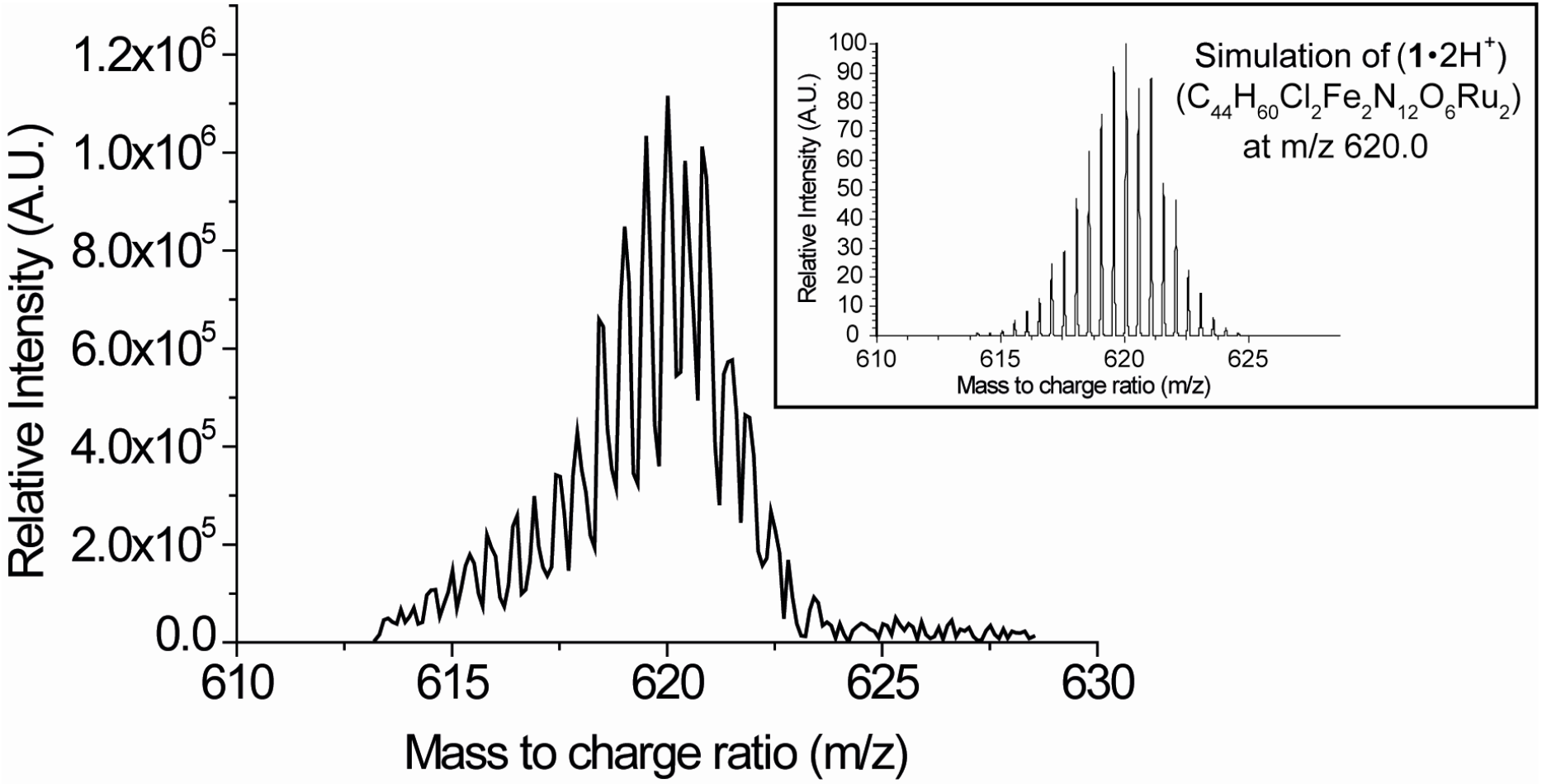

SI. Figure 1. Electrospray mass spectrum of the isotopic distribution of complex **1**: and *(inset)* its simulation of $\{[Ru(^{t}Bubpy)(CN)_4]_2–[Fe(H_2O)_3Cl]_2• 2H\}^{2+}$ peak at 620.0. The mass spectrum was performed in methanol/DMSO mixture with 0.1% of HCl.

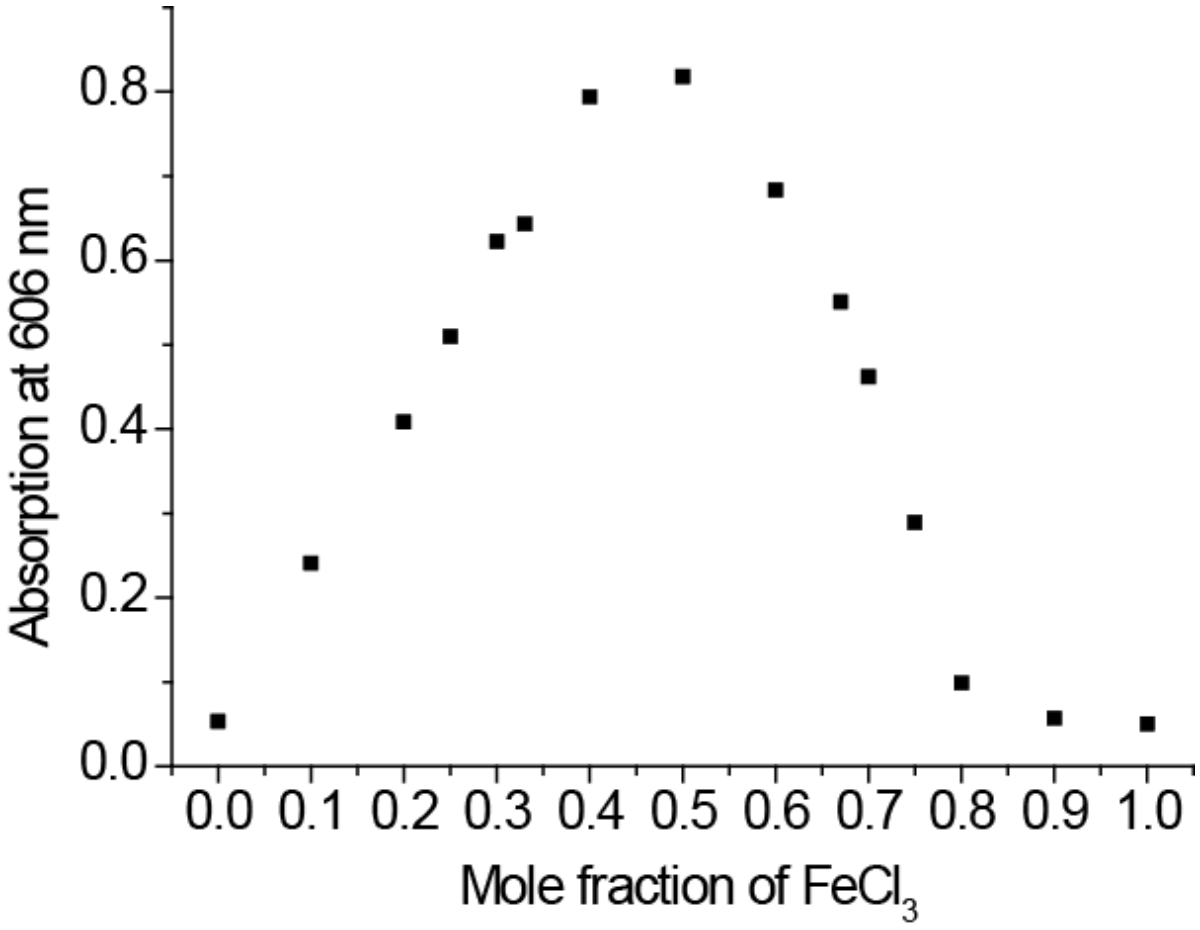

SI. Figure 2. Job's plot of $K_2Ru(^tBubpy)(CN)_4$ by $FeCl_3$ showing that the maximum response of the complex **1** occurs at amole ratio of 2:2. The experiment was performed in deionized water at 298 K.

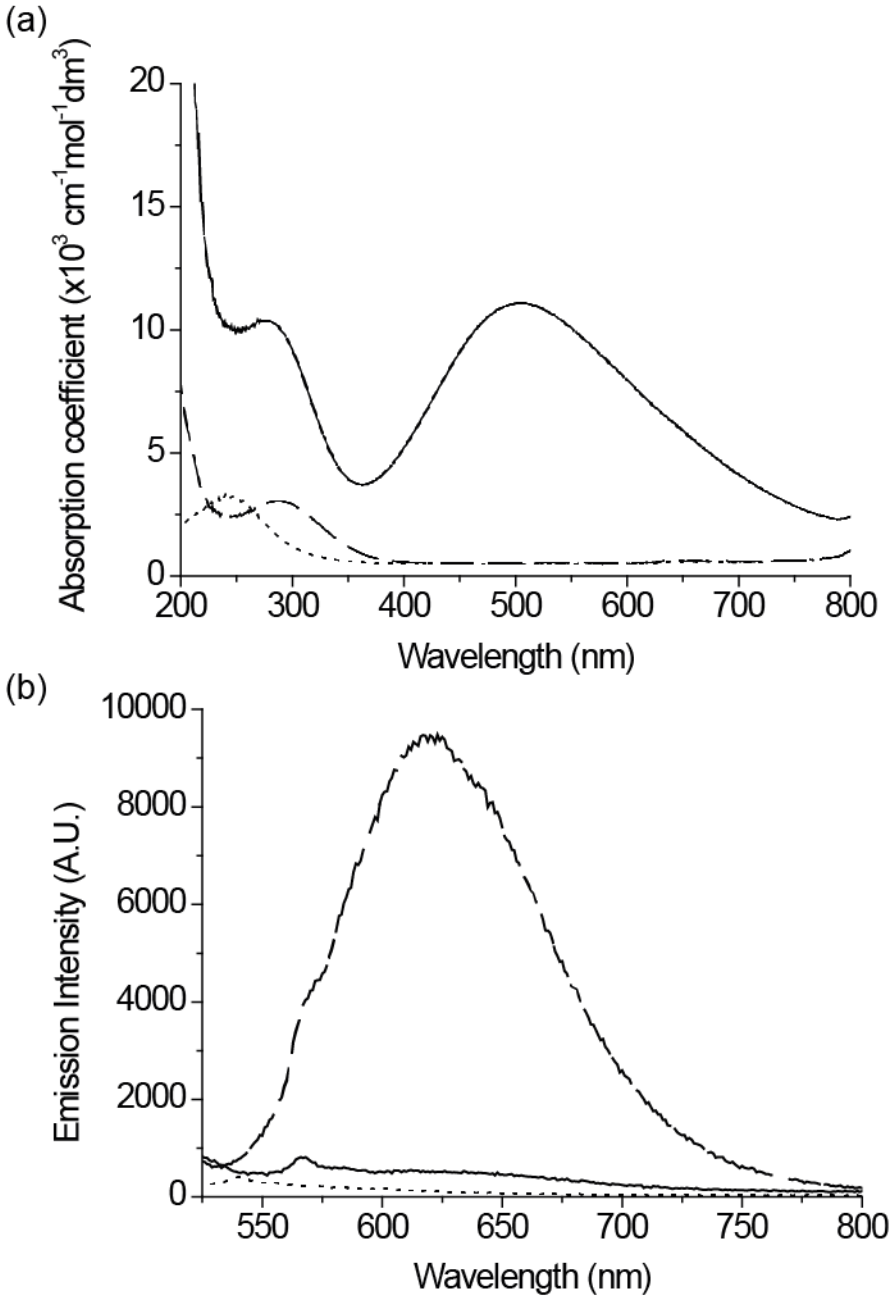

SI. Figure 3. (a) Absorption and (b) luminescent spectra of **1** (—), $K_2Ru(^tBubpy)(CN)_4$ (---) and $FeCl_3$ (···) in aqueous ethanol (1:2 v/v) (1.00 mL of aqueous KCl/HCl buffer at pH 1.5 + 2.00 mL of ethanol) at 298 K. Luminescent spectra were obtained with 467 nm excitation.

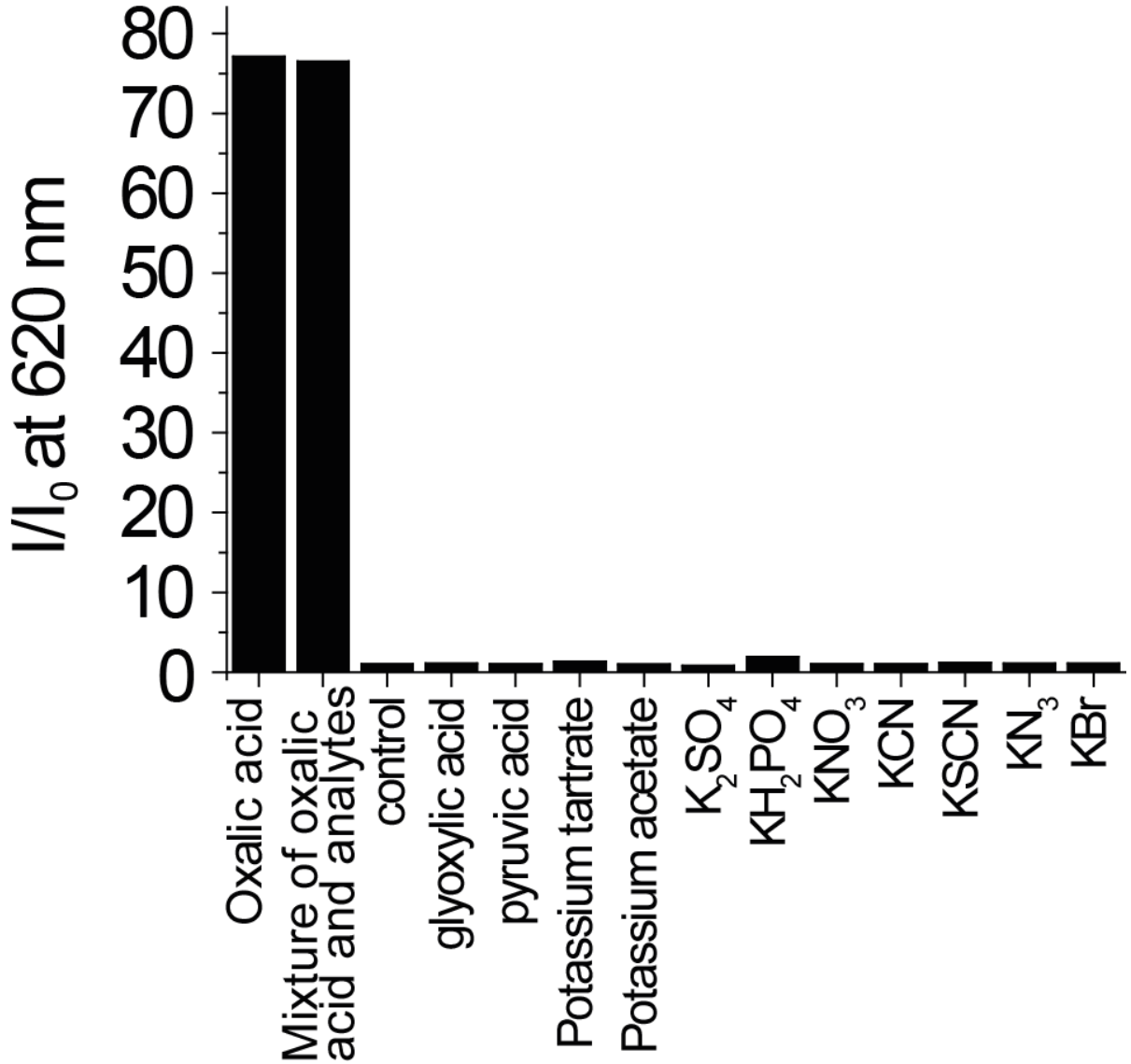

SI. Figure 4. Bar chart showing the spectrofluorometric responses of **1** (2.17×10^{-4} M) in the presence of oxalic acid and various analytes (concentration of each of the analyte 8.68×10^{-3} M: glyoxylic acid, pyruvic acid, potassium tartrate, potassium acetate, K_2SO_4, KH_2PO_4, KNO_3, KCN, KSCN, KN_3 and KBr) at aqueous ethanol (1:2 v/v) (1.00 mL of aqueous KCl/HCl buffer at pH 1.5 + 2.00 mL of ethanol) at 298 K. Luminescent spectra were obtained with 467 nm excitation.

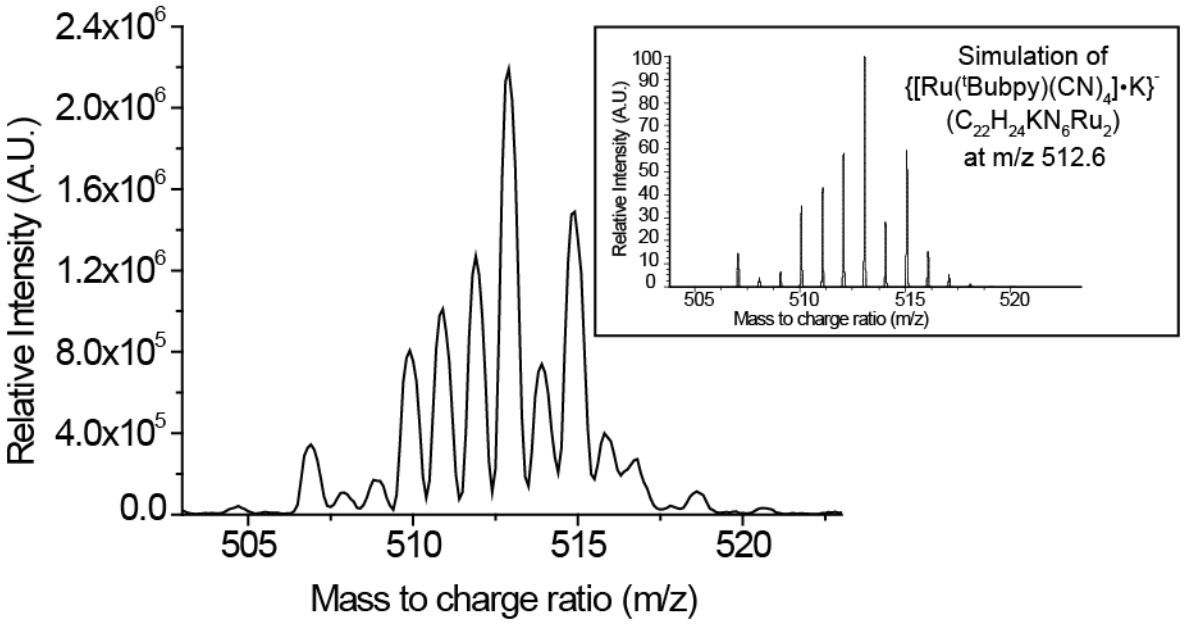

SI. Figure 5. Electrospray mass spectrum of the isotopic distribution of "**1**-oxalate-mixture": and *(inset)* its simulation of $\{[Ru(^{t}Bubpy)(CN)_4]\bullet K\}^-$ peak at 512.6. The mass spectrum was performed in methanol/water mixture.

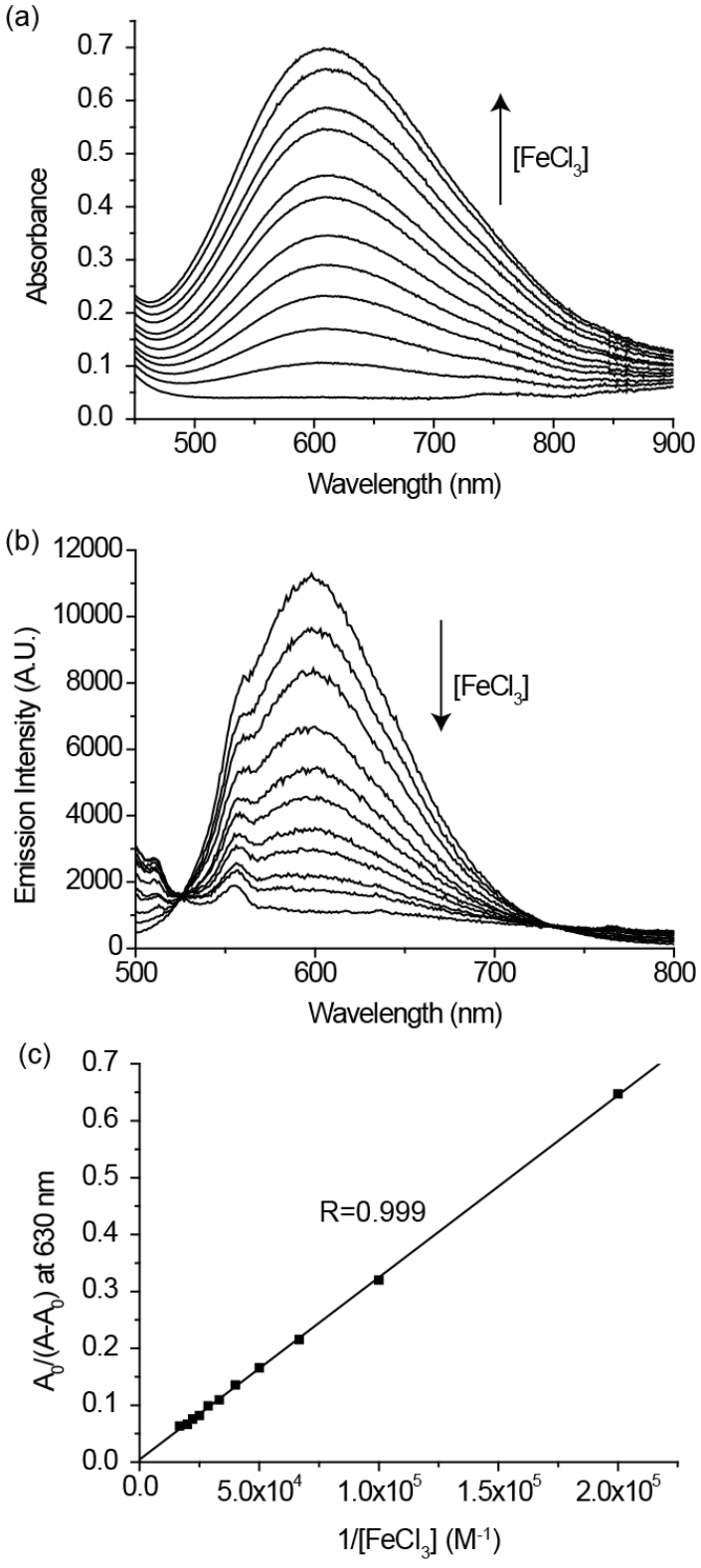

SI. Figure 6. (a) UV–vis spectroscopic, (b) spectrofluorimetric titrations of $K_2Ru(^tBubpy)(CN)_4$ (1.00×10^{-4} M) with $FeCl_3$ (0 to 1.00×10^{-4} M). (c) The slope and y-intercept are 3.20×10^{-6} and 4.56×10^{-3} respectively of the best fitted $A_0/(A\text{-}A_0)$ *versus* $1/[FeCl_3]$ plot with log $K = 3.15 \pm 0.005$ at 630 nm. All titrations were carried out in aqueous KCl/HCl buffer at pH 1.5 at 298 K. Excitation $\lambda_{ex} = 468$ nm.

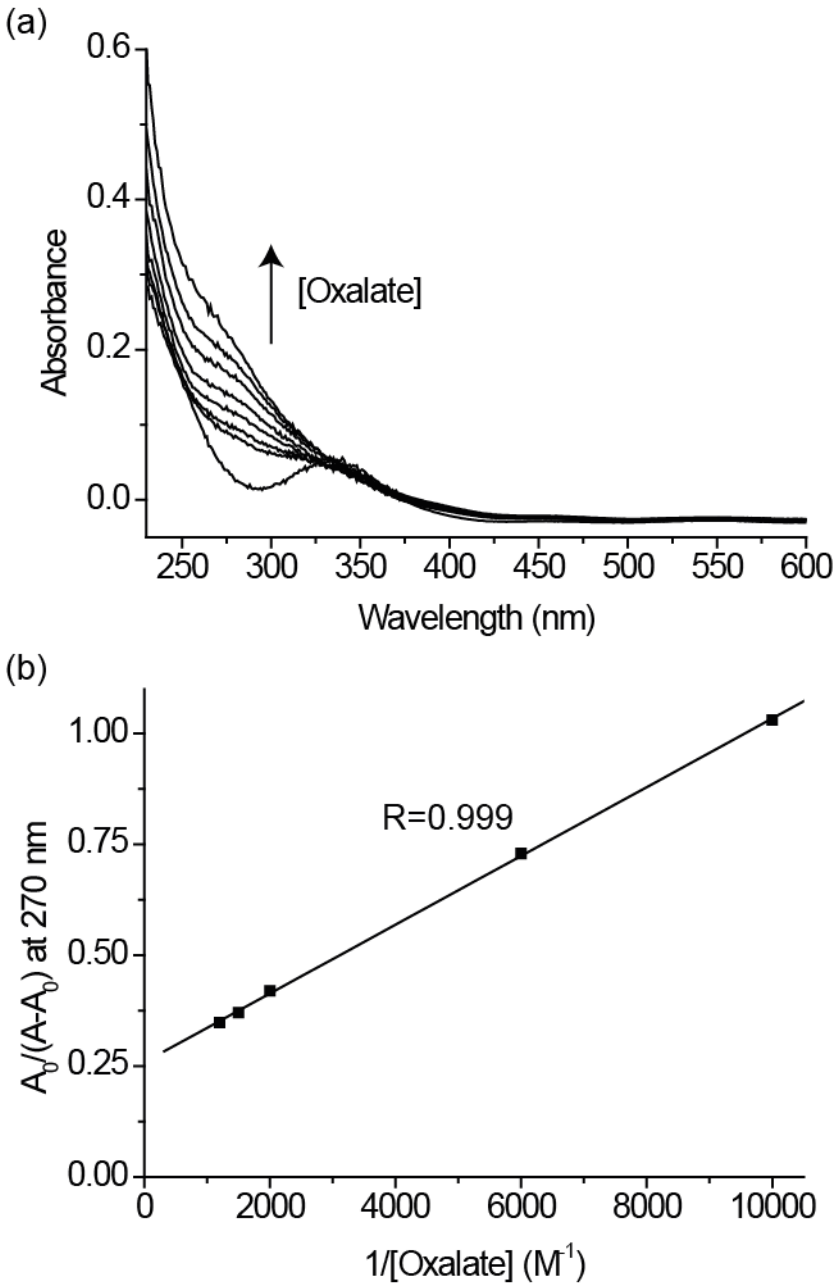

SI. Figure 7. (a) UV–vis spectroscopic titrations of $FeCl_3$ (1.67×10^{-4} M) with oxalate (0 to 1.67×10^{-3} M). (b) The slope and y-intercept are 7.75×10^{-5} M and 2.59×10^{-1} respectively of the best fitted $A_0/(A\text{-}A_0)$ *versus* 1/[oxalate] plot with log K = 3.52 ± 0.005 at 270 nm. All titrations were carried out in aqueous buffer pH 1.5 at 298 K.

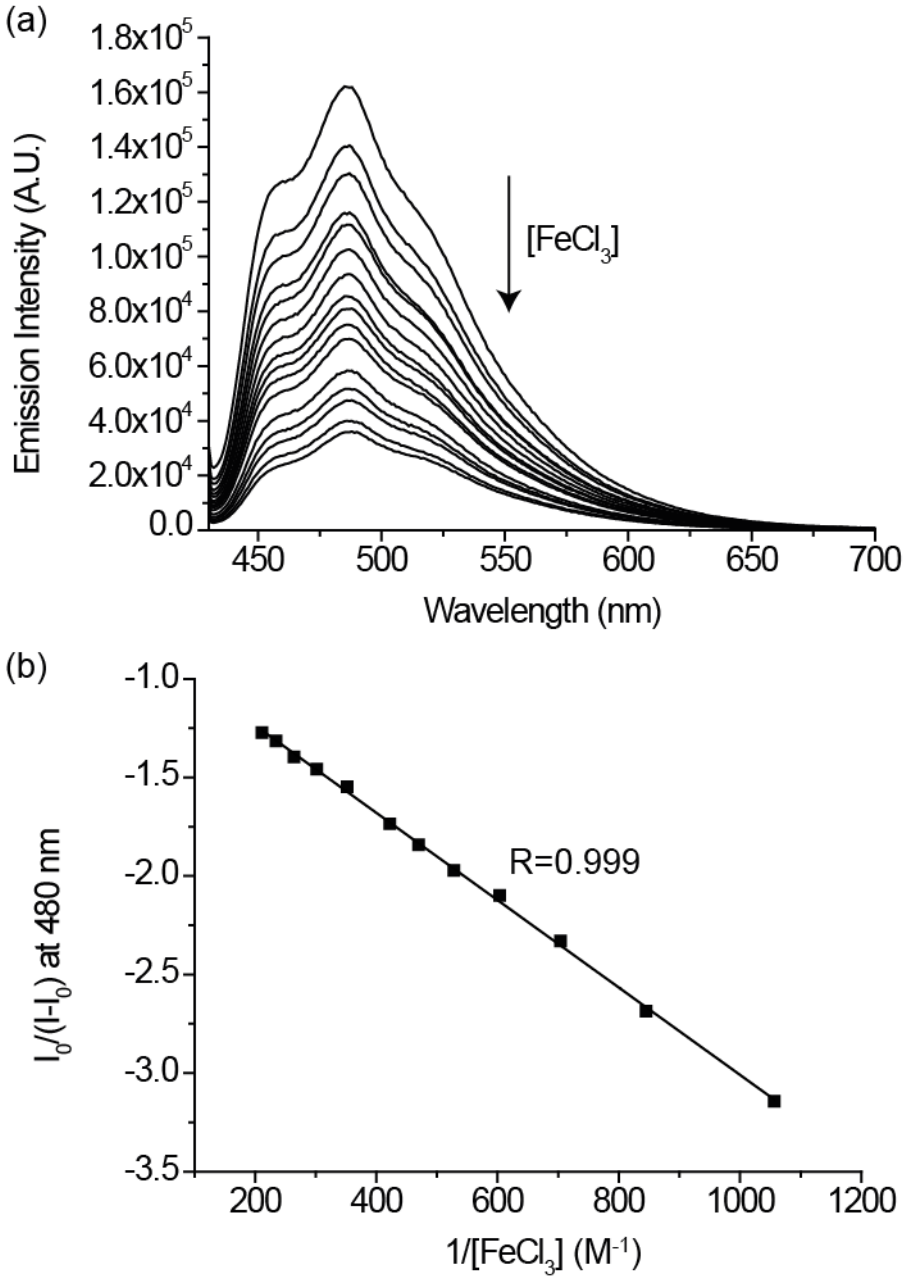

SI. Figure 8. (a) Spectrofluorimetric titrations of pyruvic acid (4.73×10^{-4} M) with $FeCl_3$ (0 to 4.73×10^{-3} M). (b) The slope and y-intercept are -2.22×10^{-3} and 7.93×10^{-1} respectively of the best fitted $I_0/(I-I_0)$ *versus* $1/[FeCl_3]$ plot with log K = 2.55 ± 0.01 at 480 nm. All titrations were carried out in aqueous buffer pH 1.5 at 298 K. Excitation λ_{ex} = 420 nm.

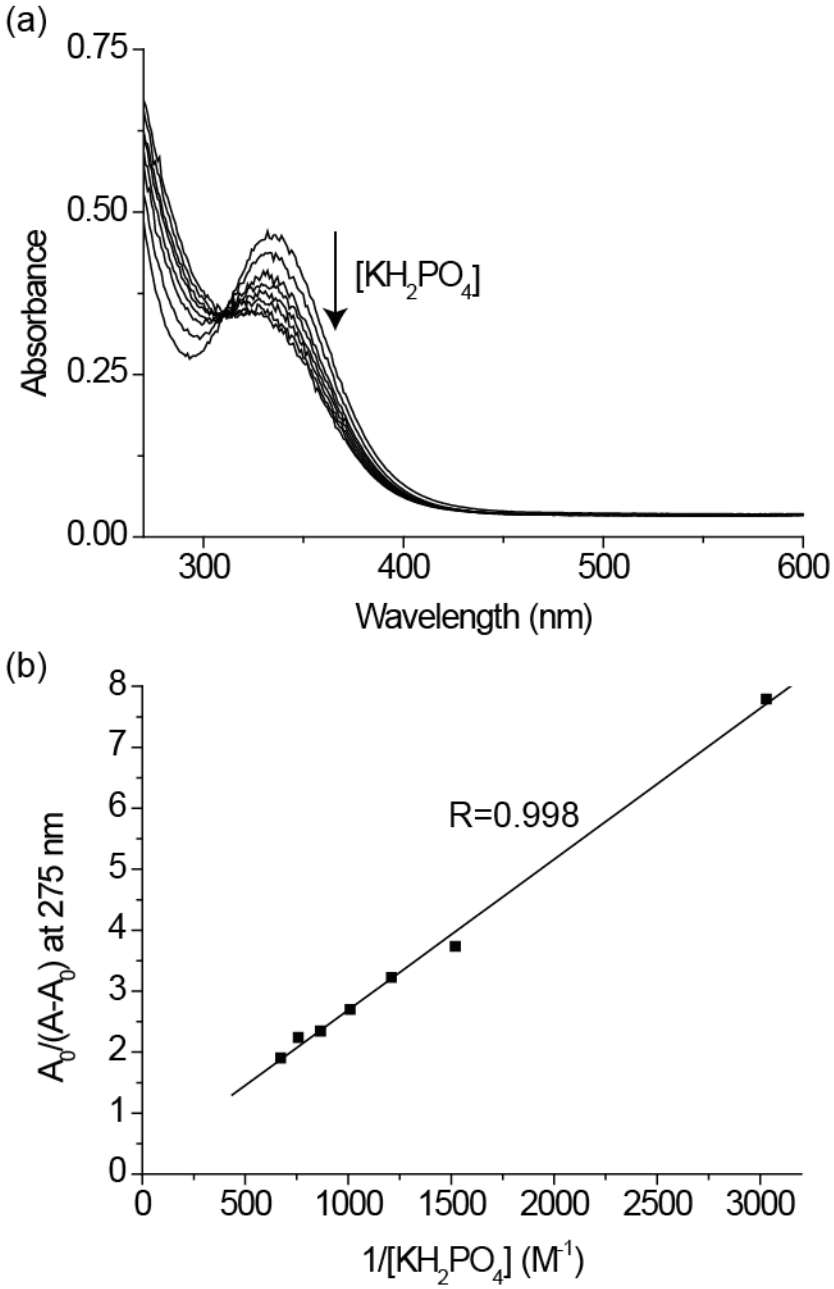

SI. Figure 9. (a) UV–vis spectroscopic titrations of $FeCl_3$ (3.33×10^{-4} M) with KH_2PO_4 (0 to 1.50×10^{-2} M). (b) The slope and y-intercept are 2.47×10^{-3} M and 5.23×10^{-1} respectively of the best fitted $A_0/(A\text{-}A_0)$ *versus* $1/[KH_2PO_4]$ plot with log K = 2.33 ± 0.02 at 275 nm. All titrations were carried out in aqueous buffer pH 1.5 at 298 K.

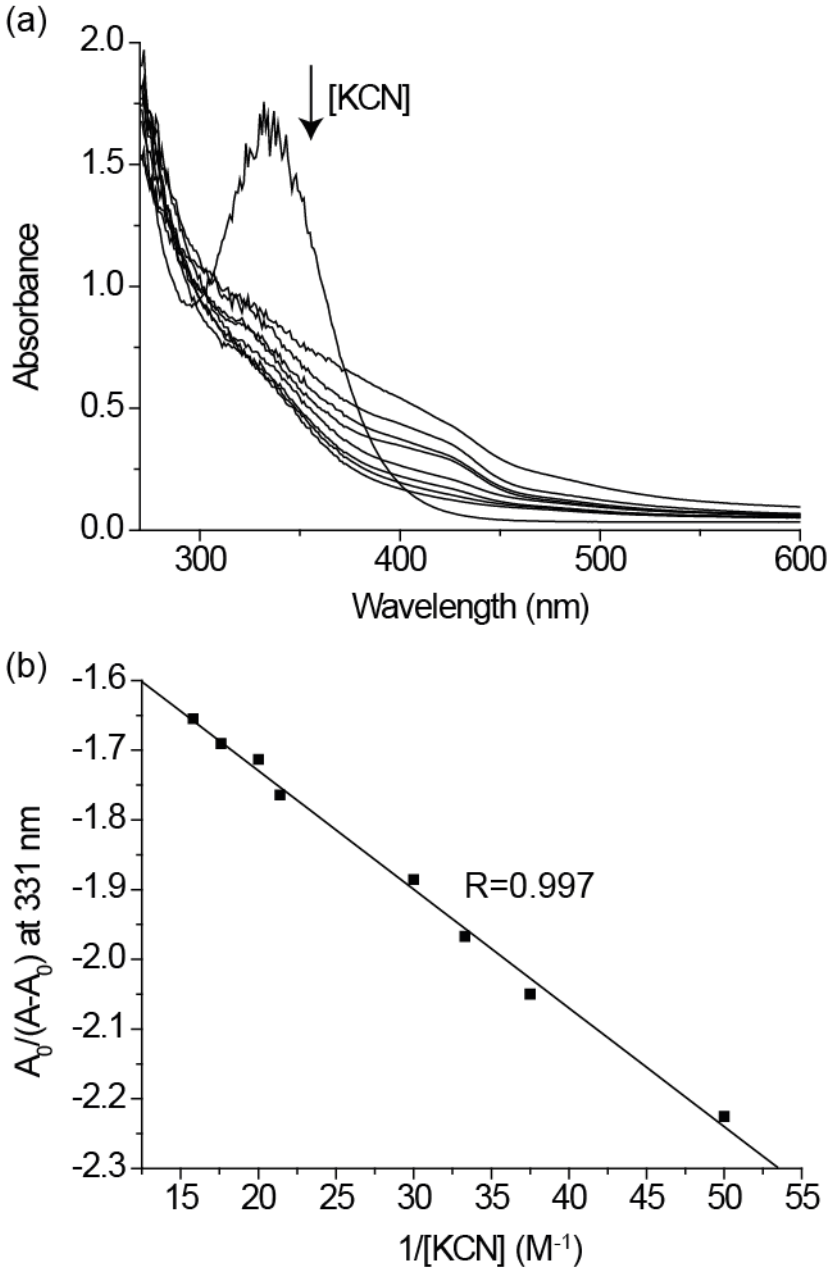

SI. Figure 10. (a) UV–vis spectroscopic titrations of $FeCl_3$ (1.00×10^{-3} M) with KCN (0 to 2.00×10^{-1} M). (b) The slope and y-intercept are -1.70×10^{-2} and -1.39 respectively of the best fitted $A_0/(A-A_0)$ *versus* 1/[KCN] plot with log $K = 1.91 \pm 0.04$ at 331 nm. All titrations were carried out in aqueous buffer pH 1.5 at 298 K.

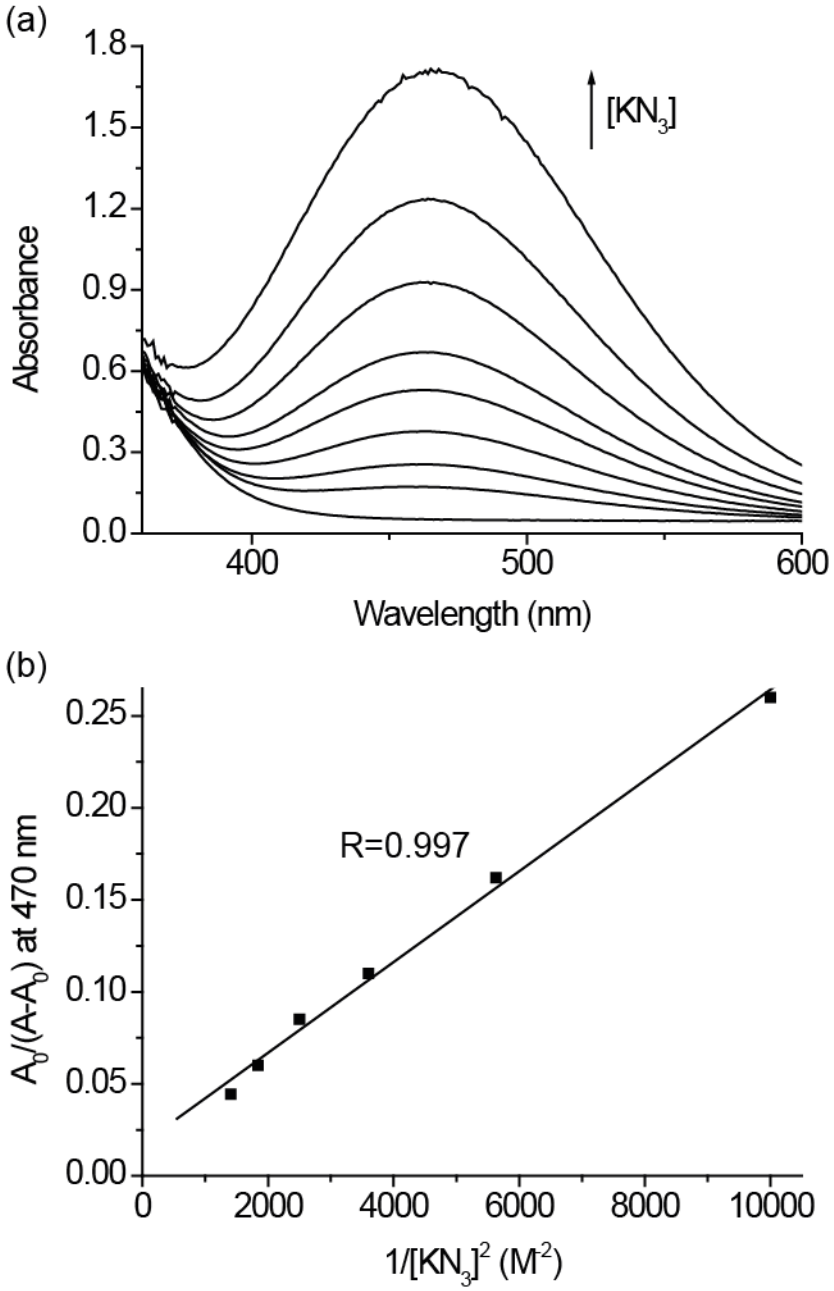

SI. Figure 11 (a) UV–vis spectroscopic titrations of $FeCl_3$ (6.67×10^{-4} M) with KN_3 (0 to 2.67×10^{-2} M). (b) The slope and y-intercept are 2.47×10^{-5} M^2 and 1.75×10^{-2} respectively of the best fitted $A_0/(A-A_0)$ *versus* $1/[KN_3]$ plot with log K = 1.43 ± 0.03 at 470 nm. All titrations were carried out in aqueous buffer pH 1.5 at 298 K.

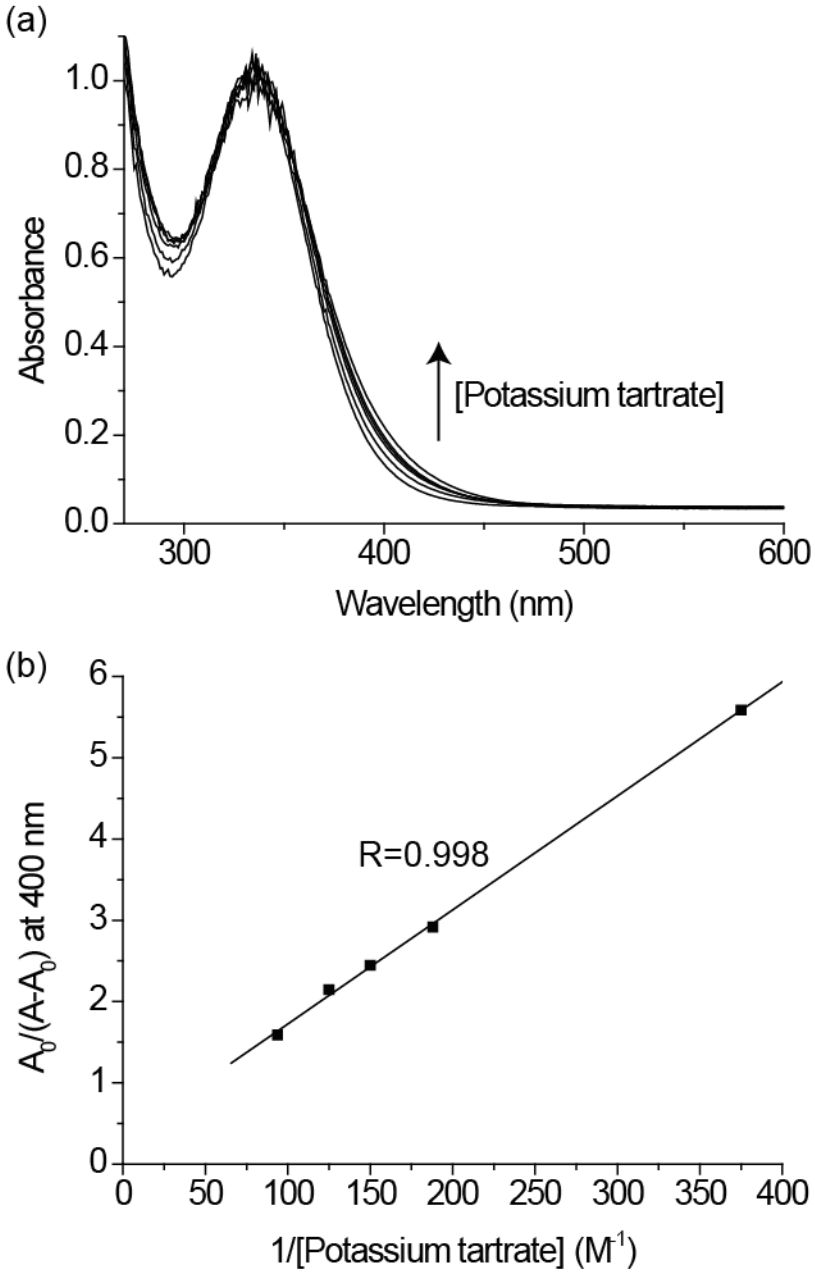

SI. Figure 12. (a) UV–vis spectroscopic titrations of $FeCl_3$ (3.33×10^{-4} M) with potassium tartrate (0 to 1.33×10^{-2} M). (b) The slope and y-intercept are 1.40×10^{-2} M and 3.23×10^{-1} respectively of the best fitted $A_0/(A\text{-}A_0)$ *versus* 1/[potassium tartrate] plot with log $K = 1.36 \pm 0.01$ at 330 nm. All titrations were carried out in aqueous buffer pH 1.5 at 298 K.

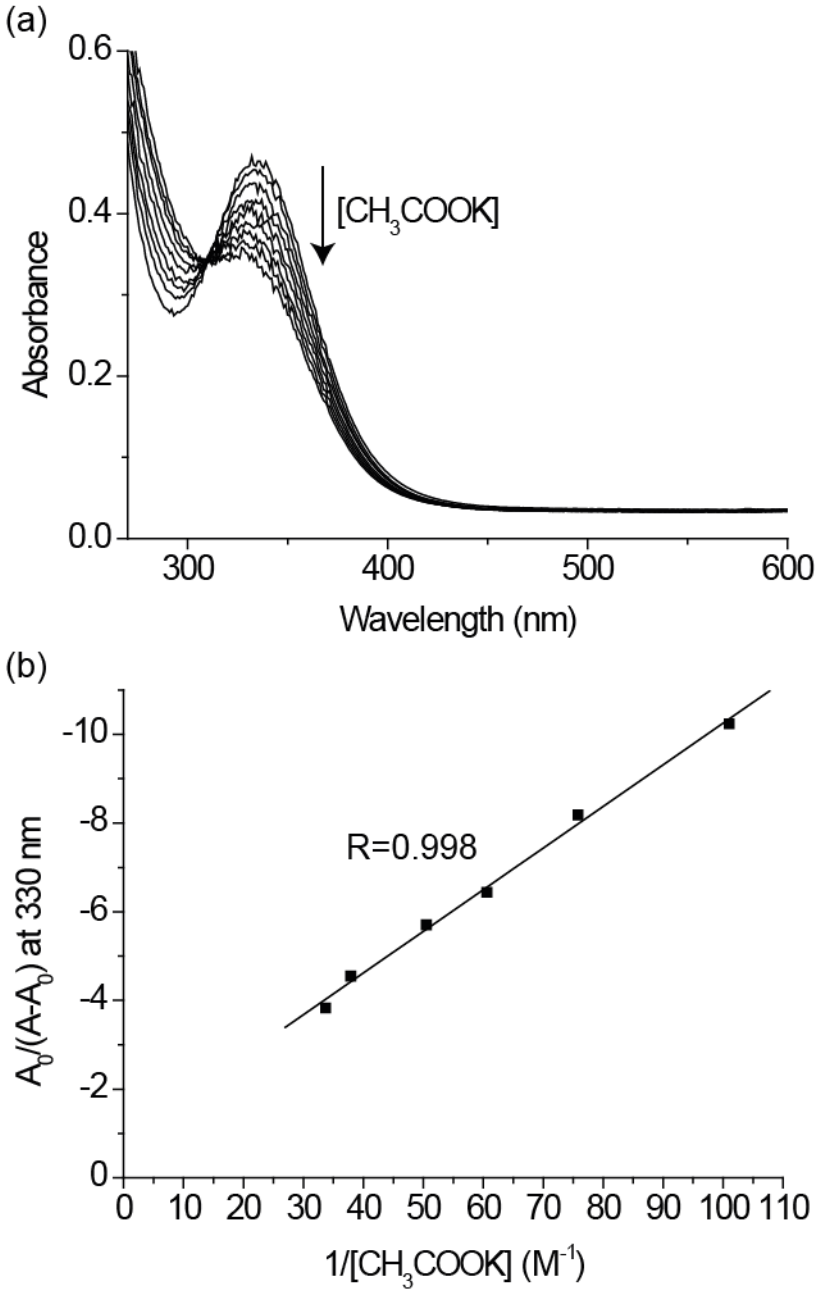

SI. Figure 13. (a) UV–vis spectroscopic titrations of $FeCl_3$ (3.33×10^{-4} M) with potassium acetate (0 to 3.33×10^{-2} M). (b) The slope and y-intercept are -9.39×10^{-2} M and -8.65×10^{-1} respectively of the best fitted $A_0/(A-A_0)$ *versus* $1/[CH_3COOK]$ plot with log $K = 0.96 \pm 0.02$ at 330 nm. All titrations were carried out in aqueous buffer pH 1.5 at 298 K.

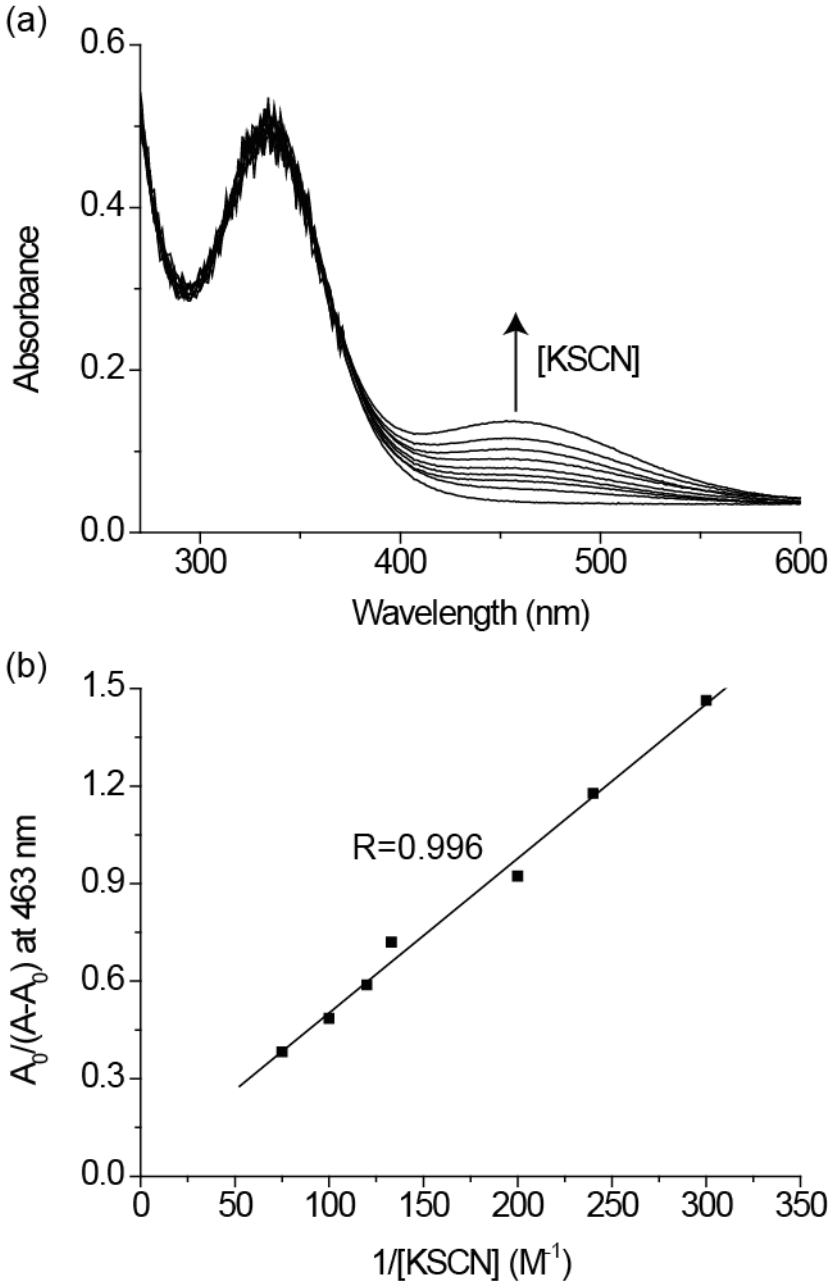

SI. Figure 14. (a) UV–vis spectroscopic titrations of $FeCl_3$ (3.33×10^{-4} M) with KSCN (0 to 1.33×10^{-2} M). (b) The slope and y-intercept are 4.75×10^{-3} and 2.69×10^{-2} M respectively of the best fitted $A_0/(A-A_0)$ *versus* 1/[KSCN] plot with log $K = 0.75 \pm 0.003$ at 463 nm. All titrations were carried out in aqueous buffer pH 1.5 at 298 K.

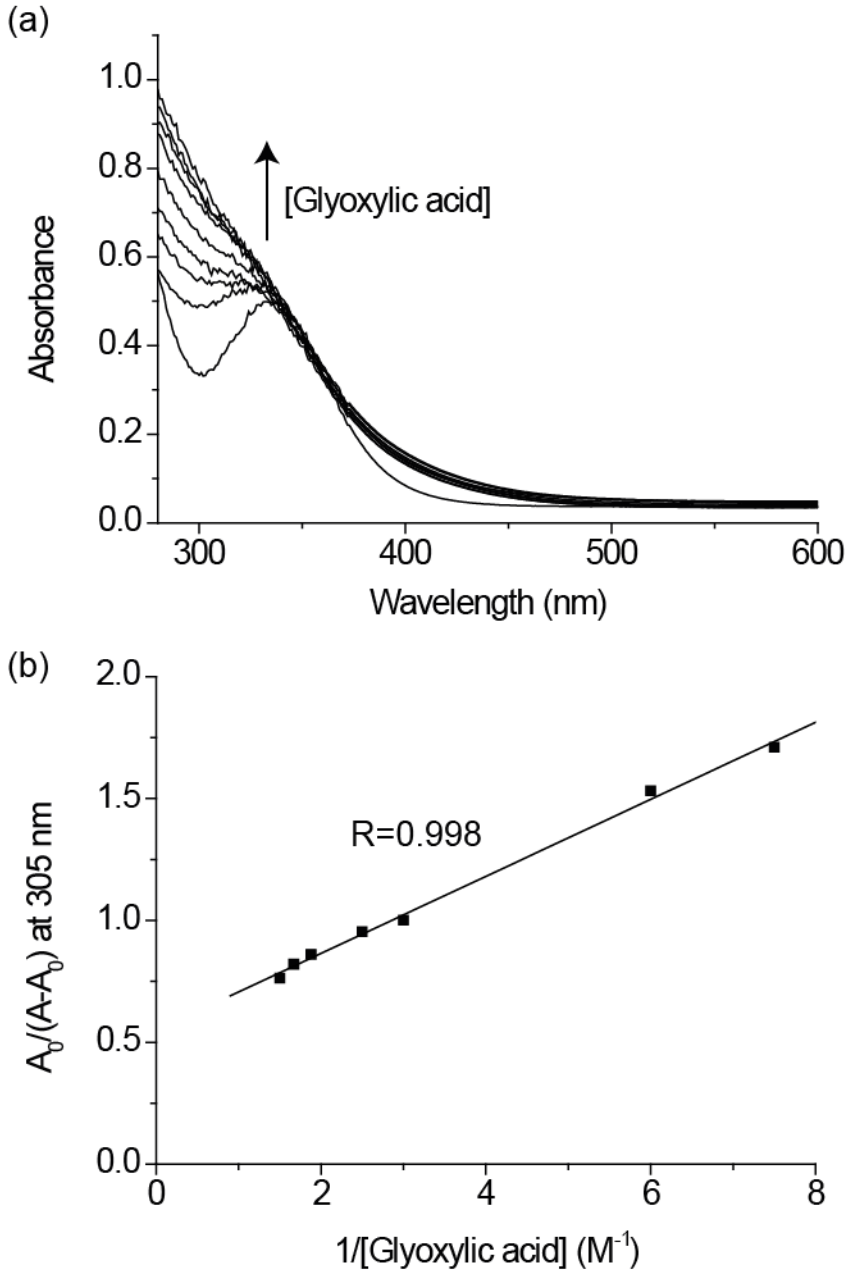

SI. Figure 15. (a) UV–vis spectroscopic titrations of $FeCl_3$ (3.33×10^{-4} M) with glyoxylic acid (0 to 6.67×10^{-1} M). (b) The slope and y-intercept are 1.58×10^{-1} M and 5.49×10^{-1} respectively of the best fitted $A_0/(A-A_0)$ *versus* 1/[glyoxylic acid] plot with log $K = 0.54 \pm 0.003$ at 305 nm. All titrations were carried out in aqueous buffer pH 1.5 at 298 K.

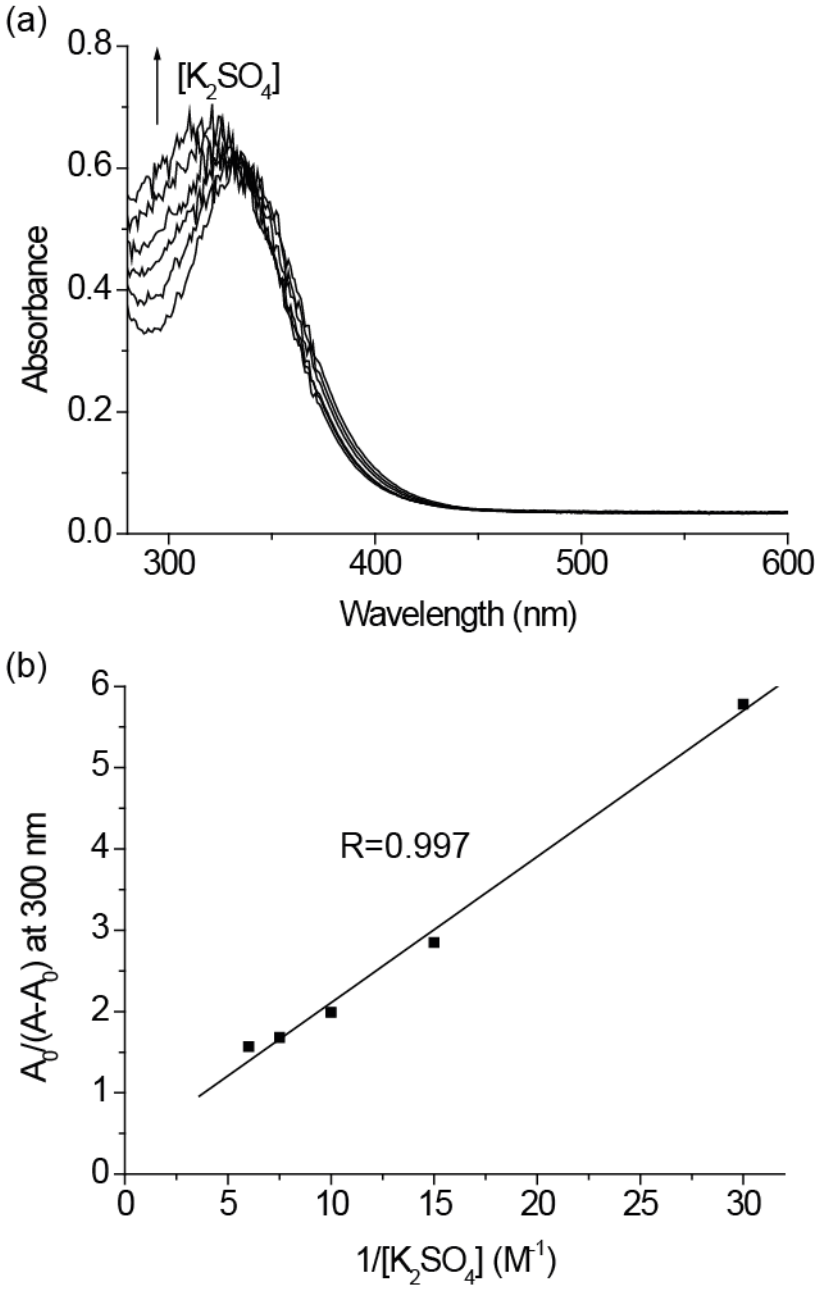

SI. Figure 16. (a) UV–vis spectroscopic titrations of $FeCl_3$ (3.33×10^{-4} M) with K_2SO_4 (0 to 1.67×10^{-1} M). (b) The slope and y-intercept are 1.80×10^{-1} and 3.11×10^{-1} M respectively of the best fitted $A_0/(A\text{-}A_0)$ *versus* $1/[K_2SO_4]$ plot with log K = 0.24 ± 0.002 at 300 nm. All titrations were carried out in aqueous buffer pH 1.5 at 298 K.

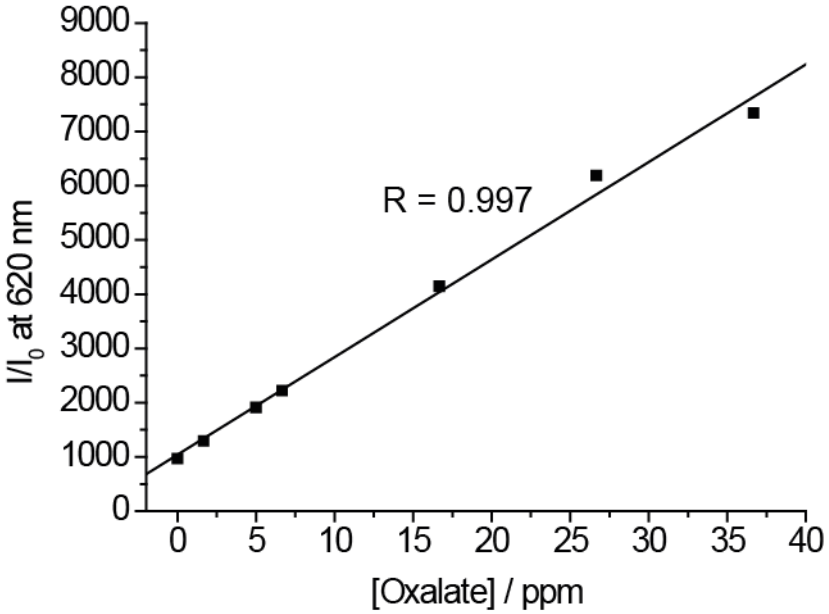

SI. Figure 17. Calibration curve developed from the spectrofluorometric titrations of **1** (3.33×10^{-5} M) with oxalate (0 to 36.67 ppm). The slope and y-intercept are 179.9 and 1041.4 ppm respectively of the best fitted I/I_0 *versus* [oxalate] plot at 620 nm. All titrations were carried out in a 2:1 ratio of ethanol/pH 1.5 aqueous buffer mixture at room temperature. Excitation λ_{ex} = 468 nm.

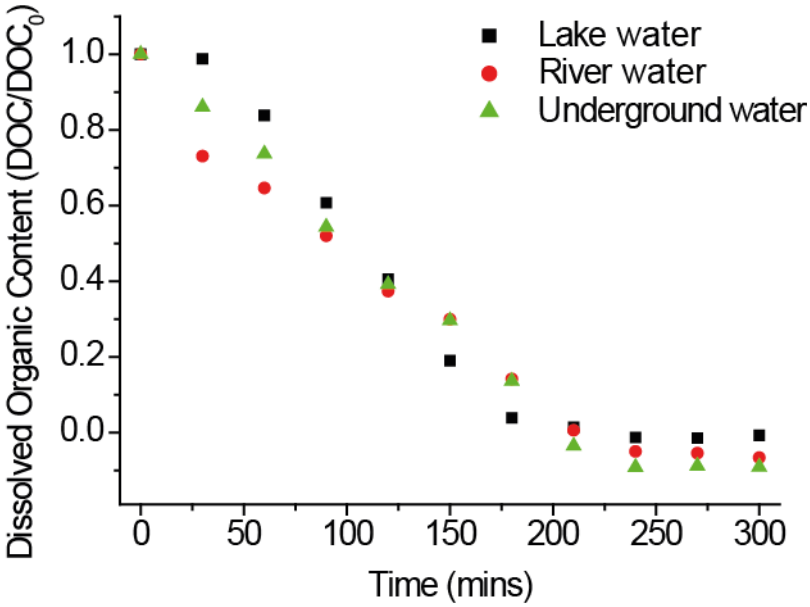

SI. Figure 18. DOC during the course of the photo-degradation of oxalate in the different water bodies within 300 min. (■) lake water, (●) river water, and (▲) underground water. All the experiments were conducted at pH 1.5 with spiked oxalate (767 ppm) under 200 Hg(Xe) irradiation at room temperature and open atmosphere.

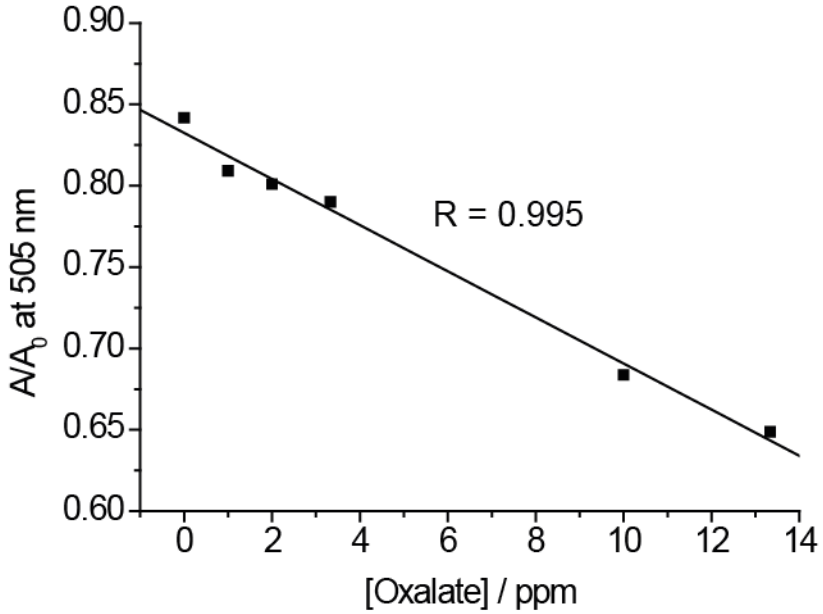

SI. Figure 19. Calibration curve developed from the spectroscopic titrations of **1** (8.61×10^{-6} M), methyl orange (1.63×10^{-5} M) with oxalate (0 to 13.33 ppm). The slope and y-intercept are -1.42×10^{-2} and 8.32×10^{-1} ppm respectively of the best fitted A/A_0 *versus* [oxalate] plot at 505 nm. All titrations were carried out in a 2:1 ratio of ethanol/pH 1.5 aqueous buffer mixture under UV-vis irradiation for 2 h.

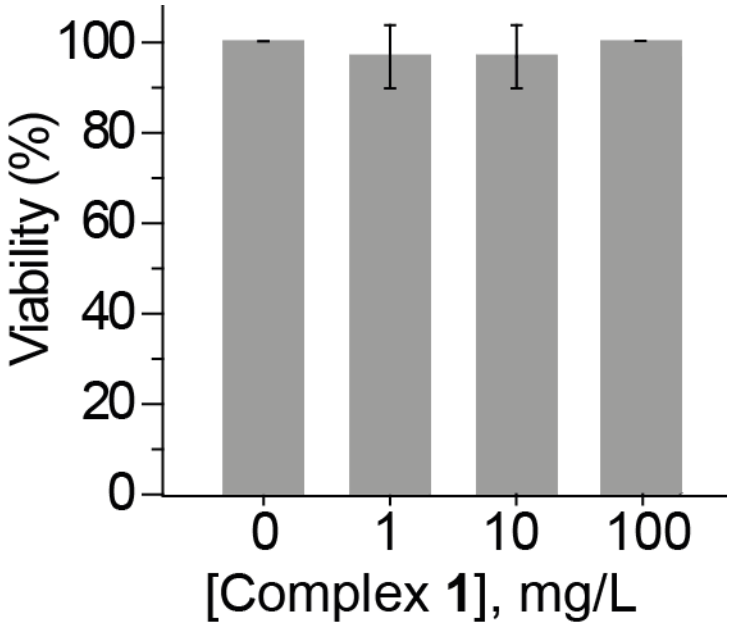

SI. Figure 20. *In vivo* toxicity studies of the the solid powders of complex **1** on Japanese medaka. Larvae were exposed to culture medium with different concentration of the solid powder from 0 to 100 mg/L, and were fed once every other day, continuously for up to 7 days.